Journal of Renewable Energy and Sustainable Development (RESD) Volume 10, Issue 2, December 2024 - ISSN 2356-8569
http://dx.doi.org/10.21622/RESD.2024.10.2.900

Received on, 23 June 2024 Accepted on, 26 August 2024 Published on, 18 September 2024

Numerical Study of a Solar PV/thermal Collector under Several Conditions in Algeria

Sihem Bouafia [1], and Mayouf Si Abdallah [2]

[1] Laboratory of Physics and Materials Chemistry, Faculty of Science, University Pole, Bordj Bou Arreridj Road, M'Sila 28000

[2] Physics Department, Faculty of Science, University Pole, Bordj Bou Arreridj Road, M'Sila 28000

sihem.bouafia@univ-msila.dz, mayouf.siabdallah@univ-msila.dz

ABSTRACT

The high temperature is known to impact the electrical efficiency of photovoltaic solar panels. The aim of this research is to suggest the utilization of hybrid panels equipped with a cooling system. The weather in M'Sila, Algeria, is extremely hot, particularly in the summer months when temperatures can soar to 50°C, which is the focus of this paper. An analysis was carried out on the efficiency of solar PV panels based on temperature and various factors such as solar radiation, ambient temperature, mass flow rate, and the temperature of inlet water used as a coolant in serpentine tubes. Iterative techniques were employed in a FORTRAN code to calculate solar radiation, system temperatures, and the efficiency of PV/T electricity generation. The numerical findings were then compared to experimental data collected by different researchers in identical circumstances. According to the numerical data, an average temperature reduction of 22°C can be attained by increasing the electrical efficiency by approximately 3.1% in an environment with a temperature of approximately 42°C, solar radiation of 1100 W/m2, and a cooling water flow rate of 300 L/h.

Index-words: *Hybrid solar panels, Solar radiation, Heat transfer, Free and forced convection.*

I. INTRODUCTION

Photovoltaic energy, a form of renewable energy, is a feasible option because of its abundance and lack of pollution, despite being expensive. Nonetheless, its usage has been on the rise because of the dwindling of traditional energy sources and limitations in resources. In addition, with the drop in production costs, it has become a viable option in the oil and gas sector. Solar energy is produced through photovoltaic technology which collects sunlight and changes it into electricity for various purposes, but some of this heat can cause solar panels to overheat, leading to a decrease in their effectiveness [1]. Many attempts have been made to find a solution for cooling photovoltaic cells and utilizing their heat by using a thermoelectric hybrid compound that combines photovoltaic and thermal modules (PV/T) for these purposes. One benefit of these substances is their capability to decrease the operational temperature of PV panels, resulting in improved effectiveness. Numerous research studies have been carried out since the 1970s to advance PV/T development.

In 2003 Ji et al. [2] conducted an analysis on the efficiency of a hybrid photovoltaic/thermal system, constructing an integrated photovoltaic/thermal system using a thermal approach. Simulation results show that the average electrical efficiencies of hybrid EPV and BPV modules are 4.3% and 10.3% per year, respectively. The annual average thermal efficiencies for hot water are 47.6% and 43.2% respectively. In 2004, van Helden et al. [3] found that the combined efficiency of PV/thermal systems is higher than the sum of the efficiencies of thermal collector systems and PV generators individually. In 2010, Da Silva et al. [4] developed a thermodynamic model for hybrid solar PV/thermal systems by utilizing a modular strategy approach within the Simulink/Matlab environment. The data that were collected show that the global efficiency is 24%, consisting of 15% thermal efficiency and 9% electrical efficiency, with an annual solar contribution averaging at 67%. In a pilot study conducted in 2013, Dube et al. [5] tested two different types of photovoltaic units to evaluate their thermal and photovoltaic performance. The initial category included a PV module with single-crystalline silicon solar cells, combined with a

Volume 10, Issue 2, December 2024 - ISSN 2356-8569
http://dx.doi.org/10.21622/RESD.2024.10.2.900

thermal collector made up of tubes and panels. The second kind was a photovoltaic panel with a thermal collector consisting of parallel plates inside, covered in polycrystalline silicon cells. The average thermal efficiency and PV efficiency for type A PVT module are 40.7% and 11.8%, while for type B they are 39.4% and 11.5%. In 2017, Nahar et al. [6] introduced a novel PVT composite layout to handle heat removal and transfer using a thermal compound, while omitting the absorber plate. This design can lower the cell temperature by up to 10.2°C.

In 2021, Walsh et al. [7] used a newer approach for SBS-PVT systems. They mixed recently developed liquids with mineral and organo imidazole along with phenanthroline derivatives. These new fluids are designed to mimic the properties of variable luminescent molecules by improving the physical and thermal characteristics of the base fluid to enhance the performance of PV treatment systems. The mixture resulted in an optical efficiency of around 63%, which was 18% to 20% higher than when using only the PV technology.

In 2022, Yan et al. [8] carried out research that utilized numerical simulations and experiments to investigate how operational factors impact cell temperature and the treatment effectiveness of PV. Findings show that a 50 L/h increase in mass flow rate caused the photovoltaic temperature to decrease from 41°C to 37.1°C, and the electrical efficiency to rise from 15.32% to 15.6%. In 2013, a numerical study on the optimal management of PV arrays was carried out by Femia et al. [9]. The study findings indicated that PV-thermal combiners are a feasible option instead of installing individual PV and thermal modules. This integration boosts efficiency by harnessing 65%–70% of the solar spectrum to generate heat and power concurrently.

In the year 2002, Trippanagnostopoulos et al. [10] conducted a study on hybrid photovoltaic/thermal solar systems. The results gathered showed that by improving diffuse reflectors to maximize both electrical and thermal energy, adding another layer of glass for better thermal efficiency, and using a combination of the two methods, the system performance could be enhanced. This enables flexibility in the design of the system.

In 2007, Tonui et al. [11] carried out research to enhance the effectiveness of solar PV/air-cooled solar collectors by utilizing forced or natural air circulation for heat extraction. The researchers aimed to enhance the general efficiency of air-cooled solar collectors by incorporating fins or slender, flat metal sheets placed either behind or within the air duct to promote increased heat exchange. This method is anticipated to greatly enhance the effectiveness of PV systems and increase their widespread adoption; fins allow for an efficiency of 30%.

In 2022, Kamazani et al. [12] investigated the technical-economic evaluation of combining ground source thermal pump (GSHP) and phase change material (PCM) with photoelectric thermal collector (PVT). The first stage of the study involved the utilization of a vertical U-type geothermal heat exchanger (GSHX) and a variable speed compressor (VSD) to conduct transient numerical simulations of ground source heat pumps (GSHP) operating in different modes (heating and cooling) using water. The utilization of the non-mainstream multi-target genetic sorting algorithm (NSGA-Sr) was implemented to enhance the levelized cost of energy (LCOE) and energy efficiency to optimize system performance. According to calculations for different scenarios, the utilization of collectors in this unified system has reduced the building total load by 6.5%. The initial scenario boasts the highest PVT energy efficiency at 53%, whereas the fourth scenario lags significantly at only 10%, resulting in a 43% difference. Totti and colleagues [13] conducted an analysis in 2023 on a numerical simulation of PVT using COMSOL Multiphysics. The study aims to increase the temperature for drying applications and then decrease the temperature of photovoltaic units to improve their electrical properties, such as power and voltage, ultimately boosting efficiency. Consequently, the temperature of the PV panel dropped from 53.37°C to 42.5°C.

In 2023, Joo et al. [14] conducted laboratory and long-term field tests to assess the overall performance and building application of liquid-based photovoltaic thermal (PVT) modules with safeguards to prevent overheating in buildings. Three types of flat photovoltaic (PV) modules have been developed and manufactured: PVT modules with transparent film covering PV cells, glazed PVT modules with glass covering PV cells, and unglazed PVT modules with glass covering PV cells. With a transparent film protecting the PV cells. Based on the thermal and electrical performance results, the PVT module with a transparent film covering the PV cells achieved a top efficiency of approximately 71.1%.

Volume 10, Issue 2, December 2024 - ISSN 2356-8569
http://dx.doi.org/10.21622/RESD.2024.10.2.900

In 2006, a research team led by K. Touafek conducted a study on a PV/T system, both with and without glass, utilizing serpentine tubes to evaluate the electrical and thermal efficiency of the prototype. The findings indicate that the hybrid panel performs better in terms of thermal and electrical efficiencies when operated without glass, achieving 70% and 60% for both models, respectively. In 2023, Ngunzi and colleagues [16] employed MATLAB Simulink to analytically explore how temperature impacts electrical efficiency for a PVT. The results from the simulation show enhancements of 16% in electrical efficiency, 20% in thermal efficiency, and 36.13% in system efficiency.

In 2023, Hamada et al [17] studied the water-based PVT system with PCM variable material capsules in both active and passive cooling modes to enhance photovoltaic panel efficiency, comparing results to a naturally air-cooled PV panel reference. The findings indicated that the PVT-PCM panel with active cooling achieved the highest increase in both electrical and thermal energy with a cooling water flow rate of 3 L/min, resulting in a total efficiency of 74.1%, which was considerably higher than the 34.6% and 12% efficiencies observed for the PVT-PCM panel with passive cooling and the standard PV panel, respectively.

In 2024, Wang and colleagues [18] examined the impact of various factors such as radiation intensity, mass flow rate, and inlet temperature on multiple PVT setups. The ideal mass flow rate is determined for locations with fluctuating solar radiation. The numeric data suggests that the electrical efficiency of a hypothetical cylindrical design grew by 1.73%, while the thermal efficiency rose by 8.29%. In 2024, Zareie et al. [19] experimentally verified the accuracy of the numerical analysis using ANSYS Fluent software for designing roll-bond (RB) in a PVT system, considering both the average temperature and temperature fluctuations across the photovoltaic surface. Under an irradiation of 1000 W/m^2, the perfect system achieves electrical, thermal, and total PVT efficiencies of 17.75%, 61.86%, and 79.56% correspondingly. In 2024, Bhutto and colleagues [20] conducted a study on how the use of the phase-changing organic material (RT-42) affected the cooling process of a photovoltaic system, utilizing the Trans programmer. When water is subjected to 440 W/m^2, it cools down at a rate of 0.45 L/min, reaching its melting point at 42°C. The results showed that inserting phase-changing materials (PT-PM) into water cooling reduced the maximum temperature of the photovoltaic cells from 59°C to 49°C. Moreover, the PVT and PVT-PCM systems both achieved a heat gain of 189 and 191 Watts, respectively. Additionally, the PV, PVT, and PVT-PCM systems had electrical efficiencies of 6.1%, 7%, and 9.5%, respectively.

This study aims to investigate the impact of climate conditions and various parameters on the electrical efficiency of photovoltaic thermal solar panels in M'Sila, Algeria. Water cooling will be utilized during three seasons to lower cell temperature and enhance electrical performance, with FORTRAN code employed for calculations. Furthermore, the goal of this research is to confirm the accuracy of the proposed computational code by comparing the outcomes to those from other researchers.

II. DESCRIPTION OF THE SYSTEM

The glass plate, solar panel, absorber plate, specially made serpentine copper tubes that use water to cool the solar panel, and a layer of insulation underneath make up the hybrid PV/T collector. Transparent TPT (Tedlar Polyester Tedlar) and EVA (ethylene vinyl acetate) cover the top side of the solar cells, while opaque Tedlar and EVA cover the bottom, as illustrated in Fig. (1). The geometrical and physical properties of these hybrid solar panels under study are presented in Tables I and II [8].

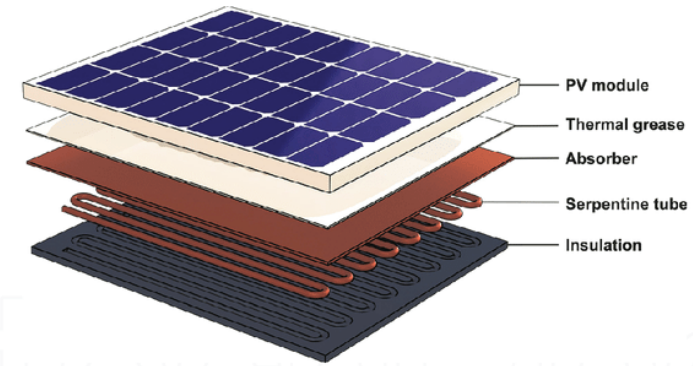

Fig. 1. The schematics of a PVT system [21]

TABLE I
HERMOPHYSICAL PROPERTIES PARAMETERS.

Components	Density (kg/m^3)	Specific Heat Capacity (J/kg.K)	Thermal Conductivity (W/m.K)
Glass	2450	500	2
EVA	960	2090	0.35
PV cell	2330	700	148
Tedlar	1200	1250	0.2
Aluminium	2719	871	202
Cooper	8960	380	380

TABLE II
GEOMETRIC PARAMETERS OF THE MODEL.

Component	Dimensions (mm)
Glass cover	1640 x 992 x 2
Aluminium absorber plate	1640 x 992 x 1.5
Water pipe inner diameter	9
Water pipe outer diameter	11

III. MATHEMATIC MODEL

A. Electrical Analysis

An equivalent model of a mono-crystalline silicon photovoltaic cell is used in this paper. It is represented by a current source to model luminous flux, a single diode with two resistors R_{sh} in parallel and R_s in series, and the model has five parameters (I_L, I_0, V_t, R_s and R_{sh}) as shown in Fig. 2. This model accurately describes the electrical behaviour of the PV module as a nonlinear device [18]. The current in this circuit can be determined directly by applying Kirchhoff law, as shown in Eq.(1), [22].

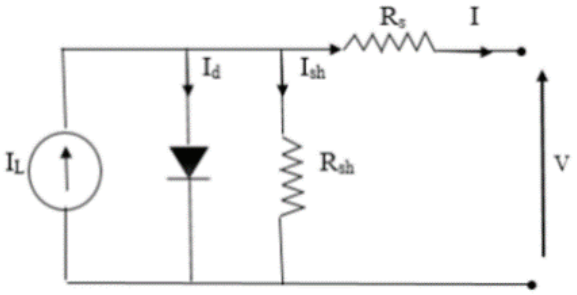

Fig. 2. Photovoltaic module

$$I = I_L - I_d - I_{sh} \quad (1)$$

Where I_L, I_d and I_{sh} represent light current, diode current, and shunt current, respectively.

$$I(V) = I_L - I_{sc}\left(\exp\left(\frac{(V+IR_s)}{Vt}\right) - 1\right) - \frac{V+IR_s}{R_{sh}} \quad (2)$$

$$P(V) = V.I = V.I_L - I_{sc}\left(\exp\left(\frac{(V+IR_s)}{Vt}\right) - 1\right)V - \frac{V+IR_s}{R_{sh}}V \quad (3)$$

Where I_{sc} is the short-circuit current and V_t is the thermal voltage of a PV module with Ns cells connected in series, and I and V are the current and voltage at load, respectively, given by:

$$V_t = k_d \frac{N_s * K * \mathrm{T}}{q} \quad (4)$$

Where q is the electron charge (=1.602x10^{-19} C), and k is the Boltzmann constant (=1.381x10^{-23} J/K); k_d the diode ideality factor and T is the cell temperature.

The hybrid module used is of type BP 585 F model, and the electrical characteristics of PV generator at standard test conditions (STC) is presented in Table III, [8].

TABLE III
ELECTRICAL PARAMETERS OF PV MODULE.

Parameter	Value
Type	Mono-crystalline silicon
Number of solar cells	60 (6 x 10)
Maximum power(W)	270
Open-circuit voltage (V)	37.99
Short-circuit current (A)	9.15
Electrical efficiency (%)	16.4
Dimension (mm)	1640 x 992

Following are the fluctuations in current and voltage at load based on differences in solar irradiation and cell temperature[23].

$$\Delta I = I(G,T_c) - I_{ref} = \beta_l(T_c - T_{c,ref})\left(\frac{G}{G_{ref}}\right) + \left[\left(\frac{G}{G_{ref}}\right) - 1\right]I_{sc,ref} \quad (5)$$

$$\Delta \mathrm{V} = \mathrm{V}(\mathrm{G},\mathrm{T_c}) - \mathrm{V_{ref}} = \beta_\mathrm{v}(\mathrm{T_c} - \mathrm{T_{ref}}) - \mathrm{R_s}\Delta \mathrm{I} \quad (6)$$

The above information is replaced to obtain the equations used to calculate the five parameters:

$$\frac{V_t}{V_{t,ref}} = \frac{T_c}{T_{c,ref}} \quad (7)$$

$$\frac{I_{sc}(T_c)}{I_{sc},ref} = \left(\frac{T_c}{T_{c,ref}}\right)^3 exp\left(-\frac{Eg\left(1-\left(\frac{T_c}{T_{c,ref}}\right)\right)}{Vt}\right) \quad (8)$$

$$I_L(G,T_c) = \left(\frac{G}{G_{ref}}\right)\left[I_{L,ref} + \beta_l(T_c - T_{c,ref})\right] \quad (9)$$

$$I_{sc}(G,T_c) = \left(\frac{G}{G_{ref}}\right)\left[I_{sc,ref} + \beta_l(T_c - T_{c,ref})\right] \quad (10)$$

$$V_{oc}(G,T_c) = V_{oc,ref} + V_t \ln\left(\frac{G}{G_{ref}}\right) + \beta_v\left(T_c - T_{c,ref}\right) \quad (11)$$

Where:

E_g: The gap energy for mono-crystalline silicon (=1,1 eV)

I_{sc}: The short-circuit current (A)

$I_{sc,,ref}$: Short-circuit current reference condition (A)

$I_{L,\,ref}$: Photonic current under reference condition (A)

V_{oc}: The open-circuit voltage (V)

G,G_{ref}: Actual lighting and reference condition (W/m^2)

T_c: is the cell temperature (K)

T_{ref}: Cell temperature at reference condition (K)

$\beta_{l,v}$: Short circuit current temperature coefficient and open circuit voltage temperature coefficient (A/K)

The open circuit voltage (V_{oc}) and the short circuit (I_{sc}) show the maximum voltage and current that the cell can supply.

Open circuit voltage: $I=0, V = V_{oc}$

Short circuit: $V= 0, I = I_{sc}$

B. The Electrical Efficiency

The electrical effectiveness of the PV/T system is the ratio between the electrical capacity generated by the cell and the photovoltaic power that it receives, so it depends on the incoming light intensity and the temperature of the cell and it is given by the following relationship [22]:

$$\eta_{el} = \frac{P_m}{GA_c} \quad (12)$$

Where P_m is the maximum power of PV/T given by:

$$P_m = V_m\, I_m \quad (13)$$

Both V_m and I_m represent the maximum effort provided by the cell, Ac is the collector area (m^2) and G is the total solar radiation rate (W/m^2).

The temperature distribution in a PV panel consisting of mono-crystalline cells is given by [24]:

$$Tpv = Te + C_t\, G \quad (14)$$

Where, Te is the ambient temperature and C_t is the proportionality factor given by:

$$C_t = \frac{NOCT(°C) - 20(°C)}{800} \quad (15)$$

The corresponding $NOCT$ parameters are total solar radiation rate

$$NOCT\ (mono) = 44°C \quad (16)$$

C. Thermal Analysis

The system description is presented in Fig. 1, the physical and geometric properties of the studied hybrid solar panel are shown in Tables I and II above.

1. The energy balance

The first law of thermodynamics forms the basis of a hybrid PVT system energy analysis. The electrical and thermal efficiency of the module over a predetermined amount of time is calculated using energy balance equations for each PV layer. The difference in internal energy is the basis for these equations, as the relationships below illustrate [25].

- ***The glass level***

The difference in internal energy between the glass cover and surrounding by convection and radiation

http://dx.doi.org/10.21622/RESD.2024.10.2.900

is:

$$m_g c_g \frac{dT_g}{dt} = h_{g-e,CV}A(T_e - T_g) + h_{g-e,RD}A(T_{sky} - T_g) + h_{g-pv,CV}A(T_{pv} - T_g) + h_{g-pv,RD}A(T_{pv} - T_g) + A\alpha_g G \quad (17)$$

- ***PV module***

The thermal equilibrium of a photovoltaic layer is expressed by the transport of heat by radiation, conduction and convection:

$$m_{pv}c_{pv}\frac{dT_{pv}}{dt} = Q_{pv-g,CV} + Q_{pv-g,RD} + Q_{pv-a,CD} + Q_{pv} - E = h_{g-pv,CV}A(T_g - T_{pv}) + h_{pv-g,RD}A(T_g - T_{pv}) + h_{pv-a,CD}A_{pv-a}(T_a - T_{pv}) + h_{pv-t,CD}A_{pv-t}(T_t - T_{pv}) + G_{irr}(\alpha\tau)_{pv} - G_{irr}r_c\eta_{EL(T)} \quad (18)$$

Where: $(\alpha\tau)_{pv}$ is the effective absorbance

The heat transfer coefficient by conduction between the adhesive layer and the tube is:

$$h_{pv-a,CD} = \frac{k_{adh}}{H_{adh}} \quad (19)$$

During photovoltaic conversion, cells convert solar radiation into electricity, and part of that radiation increases the operational temperature of the cell T_{pv}, which reduces the solar cell electrical efficiency [21].

$$\eta_{EL(T)} = \eta_{STC}\left[1 - \beta_{PV}(T_{PV} - T_{ref})\right] \quad (20)$$

- ***The plate absorber***

The thermal equilibrium at the suction layer level (absorber) is the conductive heat transfer to the PV layer, $Q_{a\text{-}e,CD}$; the heat transfer to the fluid, $Q_{a\text{-}f}$; and the heat loss to the exterior through the insulation, $Q_{a\text{-}e,CD}$.

$$m_a c_a \frac{dT_a}{dt} = Q_{a-pv,CD} + Q_{a-t} + Q_{a-i,CD} = h_{pv,CD}\left(\frac{\partial^2 T}{\partial x^2} + \frac{\partial^2 T}{\partial y^2}\right) + h_{a-pv,CD}A_a(T_{pv} - T_a) + h_{a-t,}A_{a-t}(T_t - T_a) + h_{a-i,CD}A_{a-i}(T_i - T_a) \quad (21)$$

Where:

$$A_{a-i} = A\left(\frac{W - D_0}{W}\right) \quad (22)$$

$$A_{a-t} = H_a L \quad (23)$$

$$h_{a-t} = \frac{2K_i}{X_a} \quad (24)$$

$$h_{a-i} = \frac{2K_i}{H_i} \quad (25)$$

$$x_a = \left(\frac{W - D_0}{4}\right) \quad (26)$$

Where:

A: area [m²]

L: length of the tube [m]

Ki: thermal conductivity [W/m.k]

D, H: diameter and thickness [m]

Hi: insulation thickness [m]

W: distance between two tubes

0: reference

The heat transfer coefficient to the photovoltaic layer ($h_{a\text{-}pv,CD}$) is identical in Eq. (25). It is important to note that the researchers have included the parameters $(\partial^2T/\partial x^2)$ and $(\partial^2T/\partial y^2)$ in the equation shown in Fig. 1, to accurately account for the variations in temperature of the absorber plate in the x and y directions. This is necessary due to the presence of cooling tubes under the plate absorber.

- ***Tubes***

The conductive heat transfer between the absorber plate, the PV layer, the insulating layer, and the tubes determines the energy balance for tubes.

$$m_t c_t \frac{dT_t}{dt} = h_{t-pv,CD}A_{pv-t}(T_{pv} - T_t) + h_{t-a,}A_{a-t}(T_a - T_t) + h_{t-i,CD}A_{t-i}(T_i - T_a) + h_{t-f}A_{t-f}(T_f - T_t) \quad (27)$$

Where:

$$A_{t-f} = \pi D_i L \quad (28)$$

$$A_{t-i} = \left(\frac{\pi}{2} + 1\right) D_0 L \quad (29)$$

- ***The insulation***

Due to conductive and convective heat loss, which is provided as the energy balance at the level of the insulating layer "i" accounts for the heat transfer from the absorber plate and tube to the environment.

$$m_i c_i \frac{dT_i}{dt} h_{a-i,CD} A_{a-i}(T_a - T_i) + h_{t-i,CD} A_{t-i}(T_t - T_i) + h_{i-e,CD+CV} A(T_e - T_i) \quad (30)$$

- ***The fluid***

The thermal energy released by the tube and the heat absorbed by the fluid are expressed as follows:

$$m_f c_f \frac{dT_f}{dt} = h_{t-f} A_{t-f}(T_t - T_f) + \dot{m} c_f \frac{dT_f}{dy} \quad (31)$$

Where, $\dot{m}$ (kg/s) is the fluid bulk flow rate in the tubes and (dT_f/dy) is the variation of the fluid temperature along the tube (y direction).

- ***Thermal efficiency***

The following formulas provide the PVT module thermal efficiency.

$$\eta_{th} = \frac{\dot{m} c_f (T_{fout} - T_{fin})}{A.G} \quad (32)$$

2. Heat Transfer Coefficients Expression

The coefficient of convective heat transfer ($h_{g-e'CV}$) is depending to the wind speed correlation proposed by [25]:

$$h_{g-e,CV} = \begin{cases} 5.7 + 3.8 v_W & for\ v_W < 5\frac{m}{s} \\ 6.47 + v_W^{0.78} & for\ v_W > 5\frac{m}{s} \end{cases} \quad (33)$$

The coefficient of the radiation-induced heat loss between the glass and the sky is:

$$h_{g-e,RD} = \varepsilon_g \sigma \left(T_g^2 + T_{sky}^2\right)\left(T_g + T_{sky}\right) \quad (34)$$

Where, T_{sky} is the equivalent temperature of the sky given by Swanbank's formula [25].

$$T_{sky=}\ 0.0552 T e^{1.5} \quad (35)$$

T_e: The ambient temperature (K)

ε_g: The emissivity of glass

σ: The Stefan-Boltzmann constant (σ=5.67x10^{-8} W/m^2/K^4)

By using convective heat transfer in the air gap, the thermal coefficient of the gap ($h_{g\text{-}pv,CV}$) is provided by:

$$h_{g-pv,CV} = \frac{Nu K_{air}}{b} \quad (37)$$

The air thermal conductivity is denoted by k_{air}, b represents the distance between the glass and the PV layer, and Nu is the Nusselt number determined by applying the subsequent correlations [26].

$$Gr < (1700 + 47.8\varphi) \quad Nu = 1.013 \quad (38)$$

$$Gr > 80000 \quad Nu = 2.5 + 0.0133(90 - \varphi) \quad (39)$$

Otherwise,

$$Nu = [0.06 + 3.10{-}4\,(90 - \varphi)]\, Gr^{1/3} \quad (40)$$

Gr is the Grashof number defined by:

$$Gr = \frac{g\beta\Delta T b^3}{\upsilon^2} \quad (41)$$

φ represents the collector's inclination angle in degrees and β is the thermal dilation coefficient is approximately $(1/T)$ for air.

The following formula represents the heat coefficient via radiation between a photovoltaic plate and glass:

$$h_{g-pv,RD} = \frac{1}{\frac{1}{\varepsilon_{pv}} + \frac{1}{\varepsilon_g} - 1} \sigma \left(T_g^2 + T_{pv}^2\right)\left(T_g + T_{pv}\right) \quad (42)$$

The heat transfer coefficient of the adhesive layer and the tube is:

$$h_{pv-a,CD} = \frac{k_{adh}}{b_{adh}} \quad (43)$$

The fluid heat transfer coefficient, $h_{t\text{-}f}$, is determined by the correlation process and is dependent on the

http://dx.doi.org/10.21622/RESD.2024.10.2.900

kind of flow, either turbulent or laminar [27]:

The heat transfer coefficient of the fluid, $h_{t\text{-}f}$ depends on the type of flow, whether turbulent or laminar and is defined by the following correlation [27]:

$$h_{t-f} = \begin{cases} 4.36\frac{k_f}{D_H} & for \quad Re < 230 \\ 0.023\frac{k_f}{D_H}Re^{0.8}Pr^{0.4} & for \quad Re > 2300 \\ 2\frac{k_f}{D_H} & for \quad \dot{m} = 0 \ kg/s \end{cases} \quad (44)$$

D. Assumptions and Boundary Conditions

The following boundary conditions and presumptions apply to this model:

- Different PV/T components thermal and physical characteristics under various circumstances are taken into consideration as constants.
- There is complete contact between the PV/T layers.
- The glass cover temperature is constant; the fluid inside the tube is incompressible; and the side walls of the PVT collector are considered adiabatic.
- The mass flow inlet is used as the inlet boundary; dust is not taken into consideration.
- The temperature of all components of the plate at the initial time (*t=0*) is equal to the temperature of the ambient temperature.

The boundary conditions for the absorber are:

$$(\partial^2T/\partial x^2)_{x=0} = 0 \ ; \ (\partial^2T/\partial x^2)_{x=l} = 0 \quad (45)$$

$$(\partial^2T/\partial y^2)_{y=0} = 0 \ ; \ (\partial^2T/\partial y^2)_{y=L} = 0 \quad (46)$$

Where "L" and "*l* " stand for the absorber's length and width, respectively.

The boundary conditions for the fluid:

$$(dT_f/dy)_{y=0} = 0 \quad (47)$$

IV. NUMERICAL SIMULATION

A detailed mathematical model was developed to accurately calculate solar radiation, system temperatures, and thermal and electrical efficiency. This model was created using various FORTRAN programs, specifically chosen for their effectiveness in this subject. The mathematical modeling process was crucial in developing this model.

The first program

The first program calculates the global solar radiation that reaches the PV module, considering factors such as the number of days in a year, sky conditions, and the geographical coordinates of M'Sila city.

The second program

The second program focuses on solving the heat transfer balance equations described in section (3.2). To calculate heat transfer coefficients and system temperatures, these equations are used in conjunction with boundary layer conditions. A stepwise finite difference approach was used to discretize the differential equations (17, 18, 21, 27, 30 and 31) as well as the boundary condition equations (45-47). The resulting algebraic systems were then solved using the Gauss-Seidel technique. To ensure accurate results, a convergence criterion for system temperature variables was developed. This criterion was determined by comparing the relative errors between two iterations, which were assumed to be less than 10^{-4}.

$$\left|\frac{T^{K+1}-T^{K}}{T^{K+1}}\right| \leq 10^{-4} \quad (48)$$

Where k is the number of iterations and T is the expected temperature.

Grid independence checks were performed; some calculations were made on cell temperatures using different space grids. It was found that a (200 x 300) node grid was enough to accurately model this system.

The third program

The third program is used for calculating the electric current "I" produced by a PV module. Newton's method can be used for this calculation,

Volume 10, Issue 2, December 2024 - ISSN 2356-8569
http://dx.doi.org/10.21622/RESD.2024.10.2.900

which is a widely used iterative method for solving nonlinear functions that is used to find the approximate roots of the function f(I) = 0.

Using this algorithm, the output current of a solar cell in Eq. (2) can be calculated as follows:

$$f(I) = I_L - I - I_{sc}\left(\exp\left(\frac{(V+IR_s)}{Vt}\right) - 1\right) - \frac{V+IR_s}{R_{sh}} = 0 \quad (49)$$

If the function *f(I)* satisfies the assumptions made in the derivation of the formula, then the approximation of (I_{n+1}) can be written as follows:

$$I_{n+1} = I_n - f(I_n)/f'(I_n) \quad (50)$$

Where n represents the iteration number and $f'(I_n)$ is the derivative of the current function *f(I)*.

Substituting "Eq. (49)" in "Eq. (50)", the following output current is calculated iteratively:

$$I_{n+1} = I_n - \frac{I_L - I_n - I_{sc}\left(\exp\left(\frac{(V+I_nR_S)}{Vt}\right) - 1\right) - \frac{V+I_nR_S}{R_{sh}}}{-1 - I_{sc}\frac{R_s}{Vt}\exp\left(\frac{(V+I_nR_S)}{Vt}\right) - \frac{R_s}{R_{sh}}} \quad (51)$$

The calculation should stop if this condition is checked:

$$\left|\frac{I_{n+1} - I_n}{I_{n+1}}\right| \leq \varepsilon \quad (52)$$

Where ε equal to (10^{-4}), it is the acceptable tolerance through the iteration process.

The calculation of the current I allows for the determination of the output voltage and power generated by the PV, as well as the electrical efficiency.

V. VALIDATIONS

The numerical results for the electrical efficiency and average temperature of PV cells were compared to experimental data obtained by Bin Yan et al. [8].

This comparison was conducted using a constant solar radiation intensity of 600 W/m², an inlet temperature of 25°C, and an ambient temperature of 25°C. As shown in Fig. 3a, the cell temperature decreased from 41°C to 36.9°C as the mass flow rate increased from 50 L/h to 300 L/h. This led to an increase in photovoltaic energy efficiency from 15.2% to 15.63% (Fig.3b). Additionally, the experimental results demonstrated that the temperature of the PV/T system cells decreased from 41°C to 37.1°C, while their electrical efficiency increased from 15.25% to 15.61%. This comparison highlights the close agreement between the current numerical results and the experimental results. Tables IV and V further illustrate this comparison.

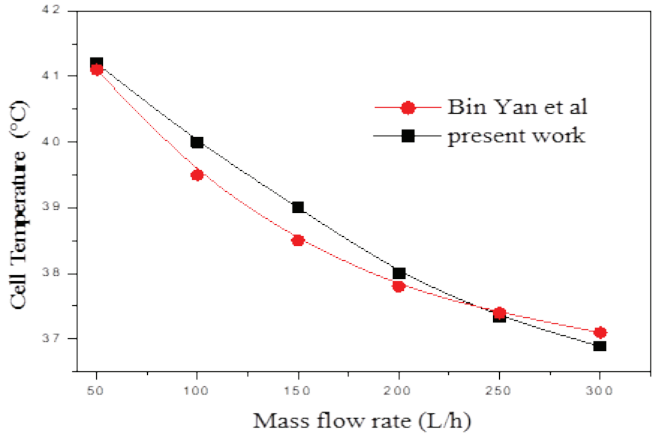

(a)

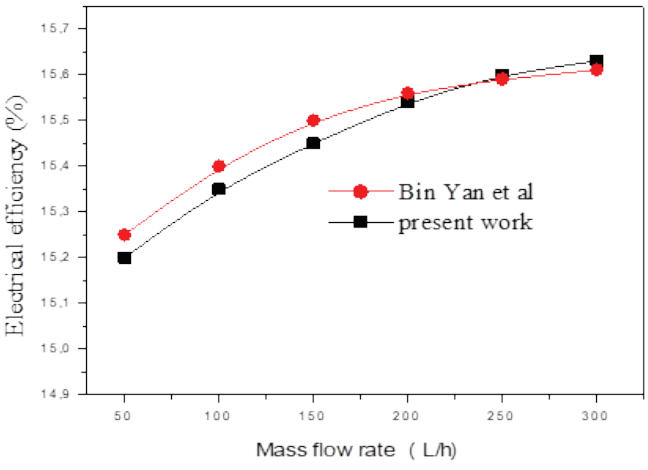

(b)

Fig. 3. Effect of the mass flow rate on: Cell temperature. (b) Electrical efficiency

http://dx.doi.org/10.21622/RESD.2024.10.2.900

TABLE IV
COMPARISON OF CELL TEMPRETURE (°C).

Mass flow (L/h)	Bin Yan et al. [8]	Present	Difference (°C)
60	41.1	41	0.1
100	39.5	40.3	0.8
150	38.5	39.5	1
200	37.8	38.5	0.7
250	37.4	37.8	0.4
300	37.1	36.9	0.2

TABLE V
COMPARISON OF ELECTRICAL EFFICIENCY.

Mass flow (L/h)	Bin Yan et al. [8]	Present	Difference (%)
50	15.25	15.20	0.05
100	15.40	15.35	0.05
150	15.50	15.45	0.50
200	15.56	15.53	0.03
250	15.59	15.60	0.01

VI. RESULTS AND DISCUSSION

A. Global Solar Radiation

Solar irradiance and sunshine duration are the two most important factors influencing PV/solar energy performance, and they are affected by geographical location and local climatic conditions.

This numerical study was conducted in the city of M'Sila (Algeria) during three seasons and on sunny days in the months of December, March, and June, corresponding to the geographical coordinates: 34.8 N latitude, 5.73 E longitude, 438 m altitude, and the PV/T panel is inclined at an angle of 30° and oriented directly towards the south (azimuth = 0°).

The researchers first compared the numerical results with the global solar radiation measured at the meteorological station in M'Sila on 21st June 2023, as shown in Fig. 4a. This comparison shows that the results are similar with minor differences; moreover, this indicates that the FORTRAN numerical code used is well suited for this calculation.

Figure 4b shows the hourly solar radiation for three seasons (spring-summer and winter), and there are significant differences between winter and spring/summer, with the intensity of solar radiation in spring/summer being almost double that of winter. However, the solar radiation intensity reaches a high value of 1120 W/m² on 21st June at 13:00, compared to other months where the solar radiation intensity reaches 800 W/m² in spring (21st March) and 550 W/m² in winter (21st December).

These variations are caused by the Earth rotation around its axis, and seasonal change is due to the Earth deviation around the Sun.

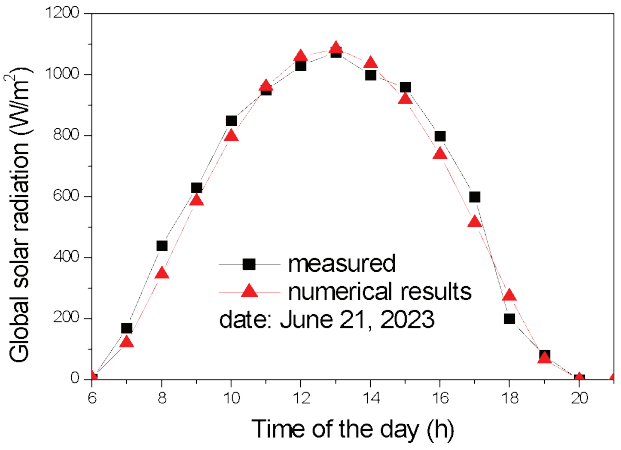

(a)

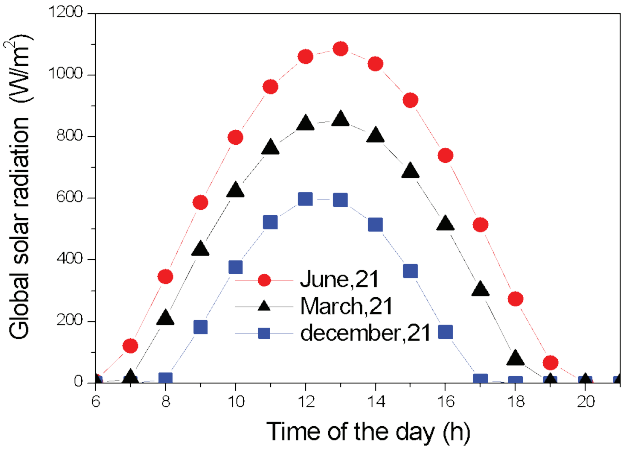

(b)

Fig. 4. Global solar radiation variation

(a): Comparison between numerical and measured results,
(b): Hourly global solar radiation for different seasons

B. Ambient Temperature

Figure 5 shows the variation of the ambient temperature during three months on sunny days. It can be observed from this figure that the ambient

Volume 10, Issue 2, December 2024 - ISSN 2356-8569
http://dx.doi.org/10.21622/RESD.2024.10.2.900

temperature reaches a maximum value of 42°C at 13.00 local time on June 21st, while the minimum of 14°C occurred on December 21st and 33°C on March 21st. These results indicate that this city is considered a hot zone during the summer season.

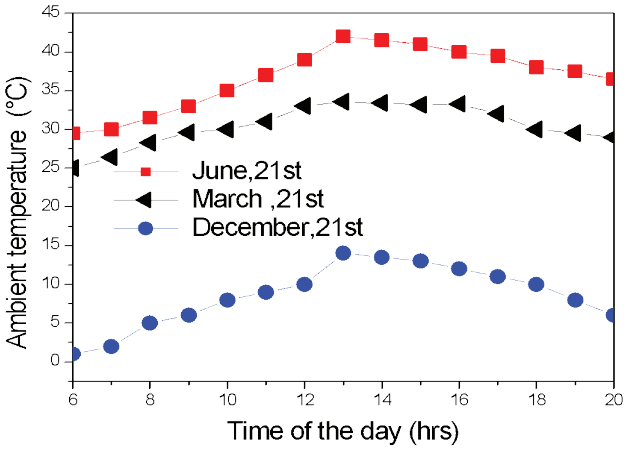

Fig. 5. Hourly ambient temperatures for different seasons

C. *Cell Temperature*

Figure 6 illustrates the effect of solar radiation and ambient temperature on the cell temperature with a constant mass flow of 300 L/h during three seasons. The cell temperature increases significantly over time with increasing solar radiation and ambient temperature, and the values at 13.00 are 53°C, 47°C, during summer and spring, respectively. It should be noted that during the month of December (winter), the mass flow rate has no effect on the temperature of the cells because the ambient temperature is so low that the photovoltaic cells do not require cooling. The researchers recall here that the calculated temperature of the cells is an average value because the temperature of the zone of the absorber in contact with the cooling tubes is lower than the temperature of the confined zone between the tubes, as shown in Fig. 7a. This average temperature is defined as:

$$T_{av} = \sum T(i, j)/((n - 1)(m - 1)) \quad (53)$$

Where:

T(i,j) is the temperature of the nod in the grid, n and m are the number of the nods on the plate absorber in the x and y directions, respectively, and (i=1, n ; j=1, m) as seen in Fig. 7b.

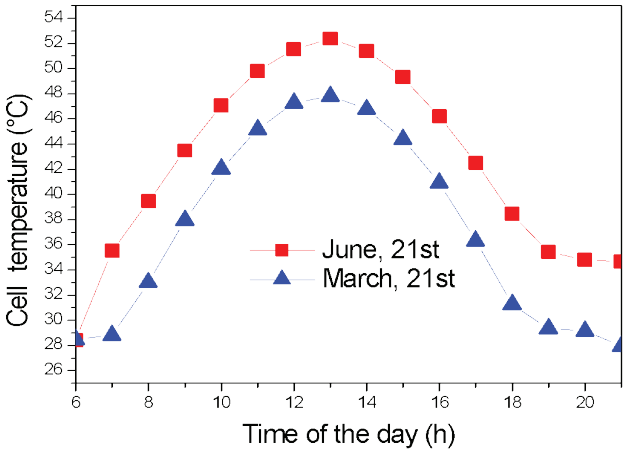

Fig. 6. Effect of solar radiation and ambient temperature on cell temperature

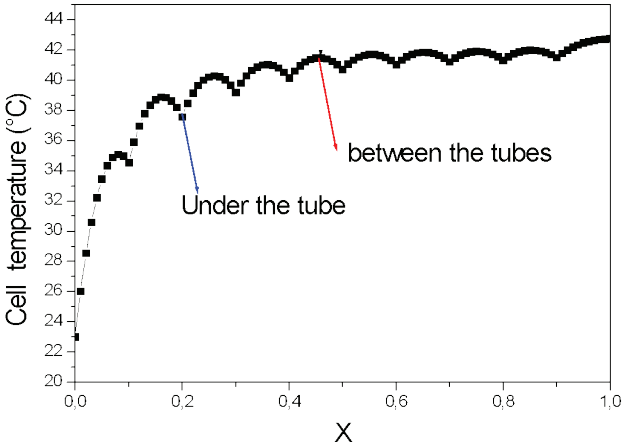

(a)

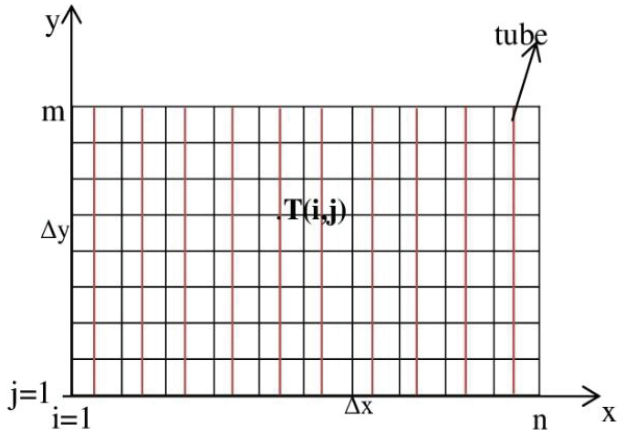

(b)

Fig. 7. (a): Cell temperature along x, (y=L/2), (b): Grid of the absorber plate

Volume 10, Issue 2, December 2024 - ISSN 2356-8569
http://dx.doi.org/10.21622/RESD.2024.10.2.900

D. Effect of Solar Radiation and Ambient Temperature on Electrical Efficiency

Figure 8 shows a significant variation in electrical efficiency values between 7.00 and 18.00 on solstice days across seasons, while maintaining a constant flow rate of 300 L/h. Electrical efficiency is highest in the early morning, regardless of day or season. Nonetheless, as ambient temperature and solar radiation rise, electrical efficiency gradually declines until 13.00, reaching its lowest values (14.90%, 13.45%, and 13%) in the winter, spring, and summer, respectively. It then rises as the ambient temperature falls in the evening.

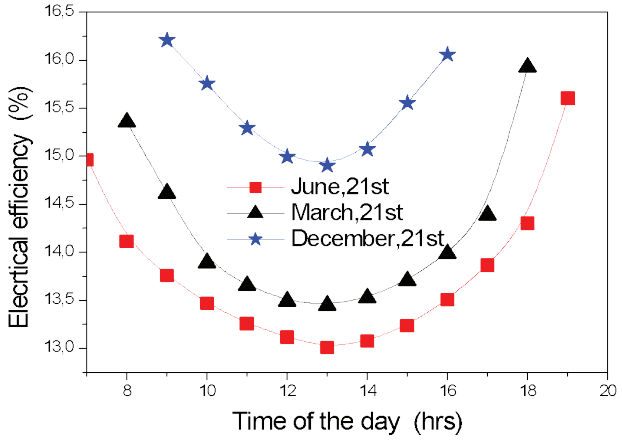

Fig. 8. Daily electrical efficiency for three days a year

E. Mass Flow Rate Effect on Cell Temperature and Electrical Efficiency

Figures 9a and 9b illustrate the impact of mass flow rate on cell temperature and electrical efficiency on June 21st at 13:00, under conditions of high solar radiation and ambient temperature. As depicted in Figure 9a) increasing the mass flow rate (q=150, 300 L/h) results in a higher coolant speed, which in turn absorbs more heat from the plate absorber. This leads to a decrease in cell temperature from 79°C to 64°C and 54.7°C, respectively. Additionally, this process leads to an increase in electrical efficiency from 9.92% to 11.83% at a mass flow rate of 150 L/h and to 13% at a mass flow rate of 300 L/h, that is, an increase of about 3.1% as shown in Fig. 9b.

This phenomenon can be explained by referring to Figures (10a) and (10b), which demonstrate that as the temperature of the solar cell increases with decreasing the flow rate, both voltage and electrical current decrease Fig.10a, resulting in lower electrical power (Fig.10b).

This is because the rise in temperature is caused by the absorption of heat energy from a portion of the solar radiation, which reduces the forbidden range of the carrier and affects the properties of the cell. The higher temperatures lead to an increase in thermal energy of the electrons. As the energy of the electrons increases, it becomes easier to break the bonds, which in turn reduces the forbidden range. Moreover, increasing the flow rate leads to increase the velocity of the liquid used in the cooling process, this effectively dissipates the excess heat and helps to maintain the cell operating temperature.

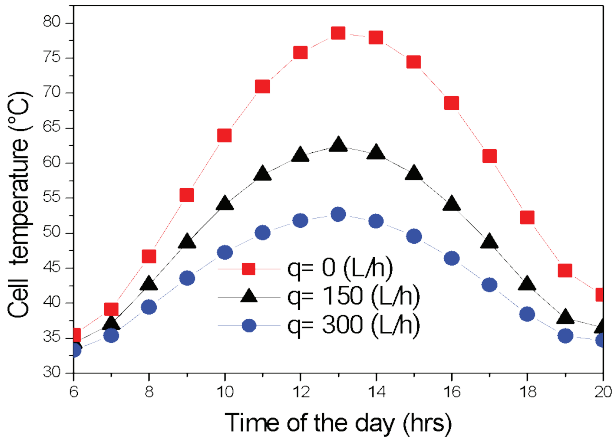

(a)

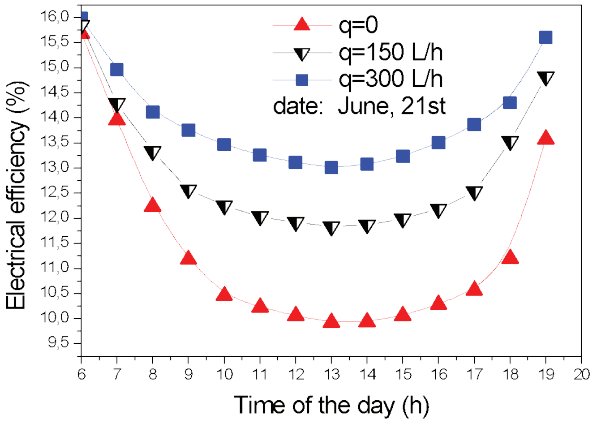

(b)

Fig. 9. Impact of mass flow rate on: (a): Temperature of the cell, (b): Electrical efficiency

Volume 10, Issue 2, December 2024 - ISSN 2356-8569
http://dx.doi.org/10.21622/RESD.2024.10.2.900

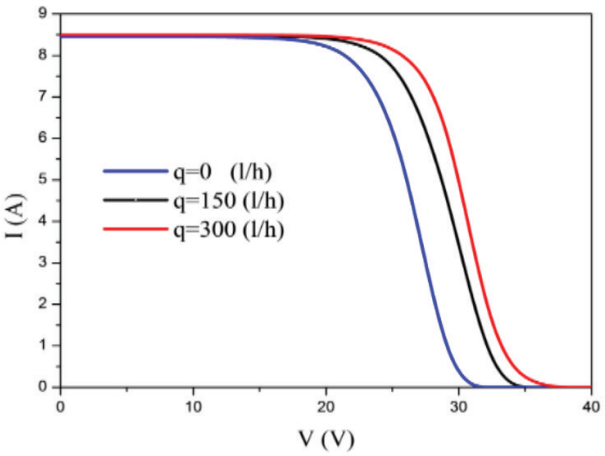

(a)

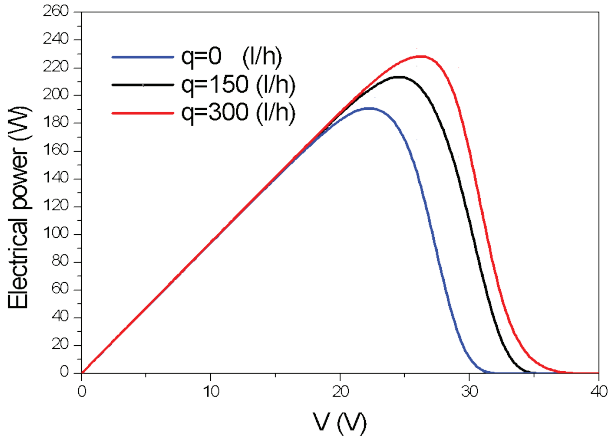

(b)

Fig. 10. Mass flow rate effect on: (a): Electrical current, (b): Electrical power

VII. PUMPING POWER

The process of cooling solar panels requires an electric pump to circulate water through the cooling pipes. This pump requires electrical energy to operate. It is assumed that the water outlet from the serpentine cooling pipes is located 2 meters above the pump. Figure 11 illustrates the energy requirements for different flow rates. For instance, at a flow rate of 300 L/h, the pump requires 1.63W or 16.3Wh of energy over a 10-hour period, which is the duration of the summer cooling process. This amount is relatively small compared to the electrical energy generated by the solar panel.

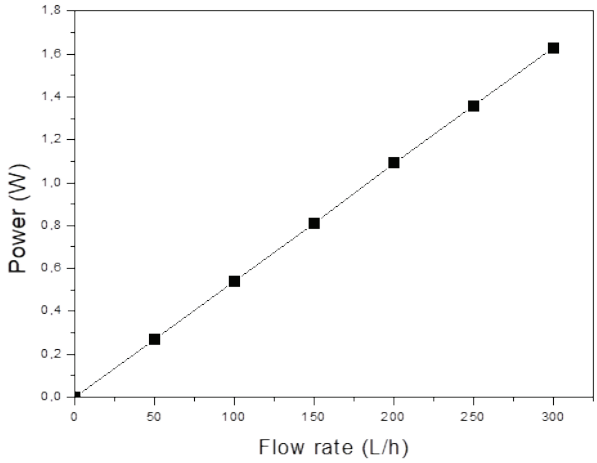

Fig. 11. Power of water pump

VIII. CONCLUSION

This study carried out a computational analysis in M'Sila, Algeria, using the FORTRAN programming code. The primary goal was to compare numerical results to experimental data from other researchers in this field. The primary goal of the study was to determine how internal and external variables affected the electrical efficiency of a photovoltaic/thermal collector using serpentine tubes and water as a coolant. To accomplish this, the computational code was validated by comparing results to those of other authors while considering variables such as ambient temperature, inlet water temperature, mass flow rate, and solar energy received by the PV cell on sunny days across three seasons. The findings suggest that M'Sila city is an ideal location for investment in this field because of its consistent sunny climate, particularly during the winter. The results show that during the summer, when solar radiation and ambient temperature are at their highest at 13:00 with a cooling flow rate of 300 L/h, the electrical yield of this type of solar panel increases by 3.1%.

This process can be applied to the solar energy station in M'sila state (Ain El-Melh), which currently produces over 20 MW of electricity. It is equipped with more than 80,000 solar panels connected to a 60 kilovolts high-voltage electricity transmission network (SPVG/T system). If the researchers implemented a cooling

system for all the solar panels in the station, with each panel increasing its efficiency by 3.1%, the total power output would be 21.86 MW, resulting in an increase of 1.86 MW. This is a significant improvement in efficiency.

Acknowledgments

The author expresses gratitude to those who helped make this research endeavour a success.

References

[1] C. Good, J. Chen, Y. Dai, and A. G. Hestnes, "Hybrid Photovoltaic-thermal Systems in Buildings-A Review," in *Energy Procedia*, 2015. doi: 10.1016/j.egypro.2015.02.176.

[2] J. Ji, T. T. Chow, and W. He, "Dynamic performance of hybrid photovoltaic/thermal collector wall in Hong Kong," *Build Environ*, vol. 38, no. 11, 2003, doi: 10.1016/S0360-1323(03)00115-X.

[3] W. G. J. Van Helden, R. J. C. Van Zolingen, and H. A. Zondag, "PV Thermal systems: PV panels supplying renewable electricity and heat," *Progress in Photovoltaics: Research and Applications*, vol. 12, no. 6, 2004, doi: 10.1002/pip.559.

[4] R. M. da Silva and J. L. M. Fernandes, "Hybrid photovoltaic/thermal (PV/T) solar systems simulation with Simulink/Matlab," *Solar Energy*, vol. 84, no. 12, 2010, doi: 10.1016/j.solener.2010.10.004.

[5] S. Dubey and A. A. O. Tay, "Testing of two different types of photovoltaic-thermal (PVT) modules with heat flow pattern under tropical climatic conditions," *Energy for Sustainable Development*, vol. 17, no. 1, 2013, doi: 10.1016/j.esd.2012.09.001.

[6] A. Nahar, M. Hasanuzzaman, and N. A. Rahim, "Numerical and experimental investigation on the performance of a photovoltaic thermal collector with parallel plate flow channel under different operating conditions in Malaysia," *Solar Energy*, vol. 144, 2017, doi: 10.1016/j.solener.2017.01.041.

[7] J. Walshe, P. M. Carron, S. McCormack, J. Doran, and G. Amarandei, "Organic luminescent down-shifting liquid beam splitters for hybrid photovoltaic-thermal (PVT) applications," *Solar Energy Materials and Solar Cells*, vol. 219, 2021, doi: 10.1016/j.solmat.2020.110818.

[8] B. Yan *et al.*, "Numerical and Experimental Investigation of Photovoltaic/Thermal Systems: Parameter Analysis and Determination of Optimum Flow," *Sustainability (Switzerland)*, vol. 14, no. 16, 2022, doi: 10.3390/su141610156.

[9] N. Femia, G. Petrone, G. Spagnuolo, and M. Vitelli, "Optimal control of photovoltaic arrays," *Math Comput Simul*, vol. 91, 2013, doi: 10.1016/j.matcom.2012.05.002.

[10] Y. Tripanagnostopoulos, Th. Nousia, M. Souliotis, and P. Yianoulis, "Hybrid photovoltaic/thermal solar systems," *Solar Energy*, vol. 72, no. 3, pp. 217–234, Mar. 2002, doi: 10.1016/S0038-092X(01)00096-2.

[11] J. K. Tonui and Y. Tripanagnostopoulos, "Improved PV/T solar collectors with heat extraction by forced or natural air circulation," *Renew Energy*, vol. 32, no. 4, 2007, doi: 10.1016/j.renene.2006.03.006.

[12] M. Abbasi Kamazani and C. Aghanajafi, "Multi-objective optimization and exergoeconomic evaluation of a hybrid geothermal-PVT system integrated with PCM," *Energy*, vol. 240, 2022, doi: 10.1016/j.energy.2021.122806.

[13] E. Touti, M. Masmali, M. Fterich, and H. Chouikhi, "Experimental and numerical study of the PVT design impact on the electrical and thermal performances," *Case Studies in Thermal Engineering*, vol. 43, 2023, doi: 10.1016/j.csite.2023.102732.

[14] H. J. Joo, Y. S. An, M. H. Kim, and M. Kong, "Long-term performance evaluation of liquid-based photovoltaic thermal (PVT) modules with overheating-prevention technique," *Energy Convers Manag*, vol. 296, 2023, doi: 10.1016/j.enconman.2023.117682.

[15] K. Touafek, A. Malek, and M. Haddadi, "Etude expérimentale du capteur hybride

photovoltaïque thermique," *Journal of Renewable Energies*, vol. 9, no. 3, 2006, doi: 10.54966/jreen.v9i3.825.

[16] V. Ngunzi, F. Njoka, and R. Kinyua, "Modeling, simulation and performance evaluation of a PVT system for the Kenyan manufacturing sector," *Heliyon*, vol. 9, no. 8, 2023, doi: 10.1016/j.heliyon.2023.e18823.

[17] A. Hamada, M. Emam, H. A. Refaey, M. Moawed, and M. A. Abdelrahman, "Investigating the performance of a water-based PVT system using encapsulated PCM balls: An experimental study," *Energy*, vol. 284, 2023, doi: 10.1016/j.energy.2023.128574.

[18] Z. Wang, G. Hou, H. Taherian, and Y. Song, "Numerical Investigation of Innovative Photovoltaic–Thermal (PVT) Collector Designs for Electrical and Thermal Enhancement," *Energies (Basel)*, vol. 17, no. 10, p. 2429, May 2024, doi: 10.3390/en17102429.

[19] Z. Zareie, R. Ahmadi, and M. Asadi, "A comprehensive numerical investigation of a branch-inspired channel in roll-bond type PVT system using design of experiments approach," *Energy*, vol. 286, 2024, doi: 10.1016/j.energy.2023.129452.

[20] Y. Ali Bhutto *et al.*, "Electrical and thermal performance assessment of photovoltaic thermal system integrated with organic phase change material," in *E3S Web of Conferences*, 2024. doi: 10.1051/e3sconf/202448801007.

[21] A. Farzanehnia and M. Sardarabadi, "Exergy in Photovoltaic/Thermal Nanofluid-Based Collector Systems," in *Exergy and Its Application - Toward Green Energy Production and Sustainable Environment*, 2019. doi: 10.5772/intechopen.85431.

[22] M. E. A. Slimani, M. Amirat, S. Bahria, I. Kurucz, M. Aouli, and R. Sellami, "Study and modeling of energy performance of a hybrid photovoltaic/thermal solar collector: Configuration suitable for an indirect solar dryer," *Energy Convers Manag*, vol. 125, 2016, doi: 10.1016/j.enconman.2016.03.059.

[23] F. Sarhaddi, S. Farahat, H. Ajam, A. Behzadmehr, and M. Mahdavi Adeli, "An improved thermal and electrical model for a solar photovoltaic thermal (PV/T) air collector," *Appl Energy*, vol. 87, no. 7, 2010, doi: 10.1016/j.apenergy.2010.01.001.

[24] M. Sardarabadi, M. Passandideh-Fard, and S. Zeinali Heris, "Experimental investigation of the effects of silica/water nanofluid onPV/T (photovoltaic thermal units)," *Energy*, vol. 66, 2014, doi: 10.1016/j.energy.2014.01.102.

[25] Hottel H. C., *Heat Transmission 3 ed William H. McAdams*, 3rd ed. New York: McGraw-Hill Book Co., 1954.

[26] F. Sobhnamayan, F. Sarhaddi, M. A. Alavi, S. Farahat, and J. Yazdanpanahi, "Optimization of a solar photovoltaic thermal (PV/T) water collector based on exergy concept," *Renew Energy*, vol. 68, 2014, doi: 10.1016/j.renene.2014.01.048.

[27] Bernard Jacques, *Énergie solaire: calculs et optimisation*. Ellipses, 2004.